npj Precision Oncology

https://doi.org/10.1038/s41698-025-01266-0

Article in Press

Ex vivo drug sensitivity profiling to complement molecular profiling in pediatric precision oncology

Received: 23 July 2025

Accepted: 23 December 2025

Cite this article as: Schoonbeek, M.C., Gestraud, P., Vernooij, L. *et al.* Ex vivo drug sensitivity profiling to complement molecular profiling in pediatric precision oncology. *npj Precis. Onc.* (2026). https://doi.org/10.1038/s41698-025-01266-0

Marlinde C. Schoonbeek, Pierre Gestraud, Lindy Vernooij, Arjan Boltjes, Vicky Amo-Addae, Marloes van Luik, Elaine Del Nery, Angela Bellini, Ellora Chua, Sarah Swaak, Eleonora J. Looze, Vilja M. Pietiäinen, Laura L. Turunen, Jani S. Saarela, Julia Schueler, Emilie Indersie, Dennis Gürgen, Katia Scotlandi, Angelika Eggert, Rachida Bouarich, Franck Bourdeaut, Sakina Zaidi, Didier Surdez, Ángel M. Carcaboso, Birgit Geoerger, Yasmine Iddir, Alexandra Saint-Charles, Elnaz Saberi-Ansari, Florence Cavalli, Apurva Gopisetty, Eva Maria Rief, Hubert N. Caron, Lou Stancato, Gilles Vassal, Stefan Pfister, Jan Koster, Selma Eising, Sander R. van Hooff, Marlinde L. van den Boogaard, Gudrun Schleiermacher & Jan J. Molenaar

Ex vivo drug sensitivity profiling to complement molecular profiling in pediatric precision oncology

*Marlinde. C. Schoonbeek[1], *Pierre Gestraud[2], Lindy Vernooij[1], Arjan Boltjes[1], Vicky Amo-Addae[1], Marloes van Luik[1], Elaine Del Nery[3], Angela Bellini[4], Ellora Chua[2], Sarah Swaak[1], Eleonora Looze[1], Vilja M. Pietiäinen[5,6], Laura L. Turunen[5], Jani S. Saarela[5], Julia Schueler[7], Emilie Indersie[8], Dennis Gürgen[9], Katia Scotlandi[10], Angelika Eggert[11], Rachida Bouarich[4], Franck Bourdeaut[12], Sakina Zaidi[4], Didier Surdez[13], Ángel M. Carcaboso[14], Birgit Geoerger[15], Yasmine Iddir[4], Alexandra Saint-Charles[4], Elnaz Saberi-Ansari[4], Florence Cavalli[2], Apurva Gopisetty[16,17], Eva Maria Rief[17], Hubert N Caron[18], Lou Stancato[17,19], Gilles Vassal[15,17], Stefan Pfister[16,17], Jan Koster[20], Selma Eising[1], Sander R. van Hooff[21], Marlinde L. van den Boogaard[1], †Gudrun Schleiermacher[4], †Jan J. Molenaar[1,22]

Correspondence in submission process should be addressed to M. C. Schoonbeek (m.c.schoonbeek-11@prinsesmaximacentrum.nl), Princess Máxima Center, Utrecht, the Netherlands

Correspondence after publication should be addressed to J.J. Molenaar (j.j.molenaar@prinsesmaximacentrum.nl; lead contact), Princess Máxima Center, Utrecht, the Netherlands

Affiliations

1. Princess Máxima Center, Utrecht, the Netherlands

2. INSERM U1331 Computational oncology, Institut Curie, PSL Research University, Mines Paris Tech, Paris, France
3. BioPhenics High-Content Screening Laboratory, Department of Translational Research, Curie Institute, Paris, France
4. RTOP (Translational Research in Pediatric Oncology), U1330 INSERM; SIREDO Integrated Pediatric Oncology Center, PSL University, Curie Institute, Paris, France
5. Institute for Molecular Medicine Finland (FIMM), Helsinki Institute of Life Science (HiLIFE), University of Helsinki FI, Helsinki, Finland
6. iCAN Digital Precision Cancer Medicine Flagship, University of Helsinki, Helsinki, Finland
7. Charles River Laboratories Germany GmbH, Freiburg, Germany
8. Xentech, 4 rue Pierre Fontaine, Evry, France
9. Experimental Pharmacology and Oncology Berlin-Buch GmbH, Berlin, Germany
10. IRCCS Istituto Ortopedico Rizzoli, Experimental Oncology Laboratory, Bologna, Italy
11. Department of Pediatric Oncology/Hematology, Charité-Universitätsmedizin Berlin, Berlin, Germany
12. Paris Cité University, Paris, France, U1330 INSERM; SIREDO Integrated Pediatric Oncology Center, Curie Institute, Paris, France
13. Balgrist University Hospital, Faculty of Medicine, University of Zurich (UZH), Zurich, Switzerland
14. SJD Pediatric Cancer Center Barcelona, Hospital Sant Joan de Deu, Sant Joan de Déu Barcelona Hospital, Institut de Recerca Sant Joan de Deu (IRSJD), Barcelona, Spain
15. Gustave Roussy Cancer Campus, Villejuif, France

16. Hopp Children's Cancer Center (KiTZ), DKFZ and German Cancer Consortium (DKTK), Heidelberg, Germany
17. ITCC-P4 gGmbH, Heidelberg, Germany
18. Hoffman-La Roche, Basel, Switzerland
19. Indiana Biosciences Research Institute, Indianapolis, United States
20. Amsterdam UMC, R2 Platform, Amsterdam, the Netherlands
21. Princess Máxima Center & Amsterdam UMC, Amsterdam, the Netherlands
22. Utrecht University, Department of Pharmaceutical Sciences, Utrecht, the Netherlands

Abstract

Pediatric patients with high-risk extra-cranial solid tumors face a 5-year survival rate below 50%. As molecular profiling alone is insufficient to guide treatment at relapse, complementary strategies like drug screening are urgently needed. We evaluated short-term drug screening as a rapid, reliable method to assess drug sensitivities in pediatric solid tumors using *ex vivo* cultures from previously established patient-derived xenograft (PDX) models. *Ex vivo* drug screening was performed within 14 days of receipt across two institutes, testing 77-224 compounds depending on cell availability. Drug responses were consistent across institutes (n=6), and effective compounds were reproducibly identified in a replicate model. Tumor type-specific responses were observed. In neuroblastoma, ALK-mutation status did not correlate with ALK-inhibitor response, whereas correlations with transcriptomic changes were observed. Timepoint-specific

drug sensitivities were observed in serial Ewing sarcoma models. Overall, drug hits were identified in 94% of screens (n=63), broadening treatment options for 88% of cases without targetable alterations (n=11). In case of a targetable event, drug screening refined compound choice. *Ex vivo* drug screening is a fast and feasible method, providing insights into compound efficacy and enabling quick identification of functional treatment suggestions. *Ex vivo* drug screening should be integrated into a future next-generation diagnostic platform for pediatric solid tumors, combined with genomics and transcriptomics.

Introduction

Although pediatric tumors are uncommon, they are the leading cause of disease-related death in children.[1] High-risk extracranial pediatric solid tumors have a poor prognosis despite intensive multimodal treatment approaches.[2] For survivors, treatment often results in severe long-term side-effects.[3] Heterogeneity in clinical response, even within cancer types, highlights the urgent need for more effective, patient-specific therapeutic approaches, based on response prediction. Currently, upon relapse or progression, pediatric precision oncology trials rely on identifying genetic biomarkers to guide clinical decisions.[4–9] However, molecular characterization alone has limitations. Actionable driver genes cannot be identified in all patients, and even when they are, responses to matched therapies are often limited.[6,7,10–12] This is partly because actionable genetic alterations do not fully capture the biological complexity of pediatric tumors.[13] Therefore, additional strategies beyond genomics are needed to guide treatment decisions.

Functional precision medicine, such as drug screening on patient-derived material, offers a promising approach to improve response prediction.[13,14] *In vivo* patient-derived xenograft (PDX) and *in vitro* patient-derived organoid models have proven effective to identify potential treatments.[10,14–17] However, establishment of these models requires extended time frames that often exceed progression-free survival of patients,[6] a limitation we also observed in our study on high-throughput screening in neuroblastoma patient-derived organoids.[18] Screening within a clinically relevant time frame would improve applicability. In addition, using *in vivo* PDX models limits the number of drugs that can be tested. *Ex vivo* drug sensitivity screening, where fresh tumor material is directly used or only shortly expanded *in vitro* before compound screening, presents such a faster alternative. Recent studies, including those from INFORM and ZERO

programs, have demonstrated the potential of *ex vivo* drug sensitivity profiling within shorter time frames, ranging from seven days to four months.[12,19,20]

We evaluated the feasibility of integrating rapid *ex vivo* drug sensitivity screening with molecular profiling, using *ex vivo* cultures from PDX-expanded pediatric tumors as tumor models. These models recapitulate molecular and phenotypic profiles of the patient tumor [16,21,22] and provide sufficient biomaterial for analysis. We demonstrate *ex vivo* drug screening using *ex vivo* cultures from PDX models as a feasible and reproducible method in a wide variety of pediatric tumors. Importantly, *ex vivo* drug sensitivity profiling of previously established PDX models can be completed within 14 days, aligning with the time frame of molecular profiling. Our findings confirmed known associations between genomic alterations and drug sensitivity, and we identified correlations between drug response and genomics, transcriptomics, and tumor growth rates. *Ex vivo* drug screening complements molecular profiling by broadening treatment options when no targetable genetic alterations are identified and refining drug selection when one or several actionable targets are present. These results support the future integration of *ex vivo* drug sensitivity profiling alongside genomics and transcriptomics within a combined diagnostic platform, aiming to improve clinical decision-making for high-risk pediatric solid tumors.

Results

Ex vivo **drug sensitivity profiling is fast, feasible and reproducible in determining drug sensitivity profiles for a broad range of solid tumors**

To perform this feasibility study of *ex vivo* drug screening in a clinically relevant timeframe, Institut Curie (Curie) in France and the Princess Máxima Center (Máxima) in the Netherlands used previously established pediatric PDXs as the pediatric tumor models. Using a comparable sample

processing and drug screening protocol at both institutes, we were able to determine drug sensitivity profiles within 14 days of PDX sample collection (Fig. 1A). We successfully performed 69 drug screens (37 in Máxima, 32 in Curie) on *ex vivo* cultures from PDX models. Screening was technically successful in 82% of cases (69/84 screens), with failures due to low viable cell yield or microbial contamination (Fig. 1B). The cohort of successful screens represent nine tumor types, including neuroblastoma (n = 26), Ewing sarcoma (n = 17), rhabdoid tumors (atypical teratoid/rhabdoid tumors and extra cerebral rhabdoid tumor samples; n = 11), rhabdomyosarcoma (n = 5), osteosarcoma (n = 4), hepatoblastoma (n = 2), malignant peripheral nerve sheath tumor (MPNST, n = 2) and synovial sarcoma (n = 2; Fig. 1C; Suppl. Fig. 1A showing center-specific cohorts). *Ex vivo* cultures were derived from PDX established from high-risk cancer patients with diverse clinical backgrounds, including untreated (at diagnosis), relapsed and progression under treatment samples. The PDX samples consisted mostly of human cells, as determined for PDX or *ex vivo* expanded samples (Suppl. Fig. 1B-C), except for a single screen (NB0537), which was therefore left out of analyses comparing drug response to genetic aberrations and gene expression.

At both institutes, drug screening was performed with libraries that include cytotoxic, cytostatic and targeted compounds (Suppl. Fig. 1D), that are either clinically approved or in (pre-)clinical evaluation to treat (pediatric) cancers (Suppl. Tab. 1-2). Depending on available PDX material, tumor cells were exposed to libraries consisting of 77 to 224 compounds, with at least 61 compounds shared across the two institutes (Fig. 1D). Drug concentrations ranged from 1e-6 to 1e3 µM, depending on the institute and the expected drug sensitivity (Suppl. Fig. 2A). Normalized area under the curves (AUC_{norm}) are used to compare drug sensitivities within a single

institute, including compounds that did not reach IC50s at the tested concentrations. However, when comparing the two different cohorts IC50 is used as AUC_{norm} values are not directly comparable due to distinct dose ranges (Suppl. Fig. 2A-B).

To assess the reproducibility of our protocol, we screened two *ex vivo* cultures from PDX models derived from the same patient at the Máxima institute. The sensitivity profiles of the two PDX screens showed a strong correlation (r = 0.95; Fig. 1E). Then, to test robustness of our method, we screened six *ex vivo* cultures from PDX models at both institutes. We observed consistent trends in drug response (r = 0.50-0.85; Fig. 1F), despite differences in PDX passage, tissue expansion time, cell seeding density, and timing of compound addition. At the Máxima, samples are cultured for seven days before drug sensitivity screening, while at Curie compound screening was immediately performed upon receipt. Overall, these findings demonstrate that despite PDX passage and protocol differences, consistent drug sensitivity profiles can be reliably determined.

To correlate the drug sensitivities with the molecular profiles and to compare *ex vivo* drug sensitivity profiling to standard molecular profiling, the PDX models were molecularly profiled using whole-exome sequencing, methylation profiling, and RNA sequencing. Targetable genetic alterations were manually curated (Fig. 1G). Across all tumors, the most common genetic alterations were pathogenic homozygous TP53-inactivation (15/69 cases), MYCN amplifications (19/69), EWS translocations (15/69) and ALK mutations (7/69). PDX models faithfully retained key genetic aberrations of patient tumors, as determined for samples of which original patient tumor profiling was available (Suppl. Fig 2C). This finding validates that our PDX models accurately reflect the genetic landscape of patient tumors. Overall, these results indicate that ex

vivo drug sensitivity profiling is feasible and reproducible for pediatric solid tumors, obtaining drug sensitivities within a clinically relevant timeframe in *ex vivo* cultures from previously established PDXs.

Ex vivo short-term profiling to identify tumor-type specific drug sensitivities

We next examined drug response patterns across tumor types by looking at the top fifteen most effective compounds, defined as those with the lowest median AUC_{norm} across all tumor types at each institute. We included the compounds tested in both institutes and find the same fifteen most effective compounds across both cohorts, supporting the consistency of drug screening trends across cohorts. These top performing compounds included the proteasome inhibitor bortezomib, chemotherapeutic actinomycin D, and BCL-2 inhibitor navitoclax (Fig 2A-B). To assess global patterns of drug sensitivity across tumor types, we performed principal component analysis (PCA) on the drug response profiles (AUC_{norm}; shown in Suppl. Fig. 3). PCA revealed partial clustering by tumor type (Fig. 2C), suggesting that while tumor type contributes to drug response, substantial inter-tumoral heterogeneity exists within types, likely reflecting underlying genetic diversity.

We then assessed which compounds showed tumor-type specific efficacy, only including tumor types where $n \geq 4$ samples were screened. Neuroblastoma samples were significantly more sensitive to the CDK4/6 inhibitor palbociclib and the MEK inhibitor cobimetinib in both cohorts ($p < 0.02$; Fig. 2D; Suppl. Fig. 4A) compared to other tumor types, altough rhabdoid tumors showed a similar but non-significant trend. Ewing sarcomas were significantly more sensitive to PARP inhibitors in both cohorts ($p < 0.002$; Fig. 2E), PARP inhibitor talazoparib was

particularly effective in Ewing sarcomas at Curie (p = 5.08E-05; Suppl. Fig. 4B). At Máxima, BRAF inhibitor vemurafenib was additionally found to be significantly effective (p = 0.002; Suppl. Fig. 4B). Rhabdoid tumors, tested at Curie, were significantly more sensitive to tyrosine kinase inhibitors ponatinib and axitinib (p < 0.002; Suppl. Fig. 5). Osteosarcoma, a tumor type that is difficult to model *ex vivo* and in urgent need of new treatment options,[23] was broadly resistant to most compounds compared to other tumor types (Suppl. Fig. 6), including for instance talazoparib (Suppl. Fig. 4B). For rhabdomyosarcoma, no compounds or drug classes showed significant efficacy compared to other tumor types (Suppl. Fig. 6-7). However, low sample sizes for osteosarcoma and rhabdomyosarcoma (n = 4) limit robust conclusions. Taken together, these results provide initial data on compounds with broad efficacy and tumor type-specific drug response trends.

Genetic aberrations alone poorly associate with *ex vivo* drug response

To assess the predictive value of molecular profiling, we first confirmed the known association of resistance to MDM2-inhibitor idasanutlin and XPO1-inhibitor selinexor upon homozygous TP53-inactivating mutations.[24–27] Samples with homozygous TP53-inactivation were significantly more resistant to the MDM2 inhibitor idasanutlin (p < 0.002; Fig. 3A), and selinexor (p < 0.039; Suppl. Fig. 8A) compared to TP53 wild type or heterozygous TP53-inactivated samples.

We then explored whether targetable genetic alterations predicted drug sensitivity across tumor types, focusing on compounds targeting these alterations (Suppl. Tab. 3). Beyond TP53, only 3 out of 22 (Máxima) and 1 out of 15 (Curie) showed any significant association with response to their matched compound (Fig. 3B; Suppl. Fig. 8B). None of these associations were

shared across cohorts. In Máxima, significant associations involved MYCN amplifications and ALK alterations, which are neuroblastoma specific. None of the associations observed across the pan-cancer cohort remained significant when this analysis was restricted to neuroblastoma, suggesting the correlations were confounded by tumor-type rather than the genetic alteration themselves (Suppl. Fig. 8C). All in all, these findings suggest that genetic aberrations alone are not sufficient to predict *ex vivo* drug response.

Ex vivo growth rate of tumor samples as a quality control metric

For the screens performed in the Máxima cohort, growth rate was determined by comparing cell viability at t = 0h and t = 72h in untreated controls, to assess screen quality and evaluate its impact on drug sensitivity. Growth rates of the included screens ranged from 60% to 479% (mean = 179%; Suppl. Fig. 8D), with values below 100% indicating spontaneous cell death and those above 100% representing proliferation. Screens with a growth rate <60% (n= 2) were excluded at an earlier stage and marked as failed (Fig. 1C). All four osteosarcoma screens, a tumor type that is generally hard to culture *ex vivo* [23], had growth rates above 100% (mean = 177%). For the full cohort, sensitivity to 24 compounds correlated significantly with growth rate (Suppl. Fig. 9A), particularly cytotoxic and cell cycle-targeting agents such as CHK1 inhibitor prexasertib, the tubulin inhibitor docetaxel (Fig. 3D), gemcitabine and topoisomerase inhibitor camptothecin. These associations confirm their known mechanism of action and validate growth rate as a relevant quality control parameter in *ex vivo* drug screens.

Serial _ex vivo_ models illustrate tumor progression and shifting therapeutic windows

To explore whether drug sensitivity may change during tumor progression, and to explore the potential added value of screening drug sensitivities at multiple timepoints, we analyzed serial models from two Ewing sarcoma patients screened in the Máxima. While overall similarity was observed between primary tumor (treatment-naive) and progression under treatment samples, (ES0482: r = 0.78; ES0619: r = 0.72; Fig 3E), distinct timepoint-specific sensitivities were found. For ES0482, the sample obtained at progression resembled the primary sample genetically (Fig. 1G), yet was generally slightly more sensitive. Higher sensitivity of topoisomerase and tubulin inhibitors in the sample from progression (Fig. 3E), could be explained by the higher growth rate (primary: 172%; progressed: 314%) (Suppl. Fig. 9A). The progressed sample of ES0619 acquired a homozygous TP53 inactivating mutation and was resistant to idasanutlin (IC50 = 0.8 µM in primary versus not reached in progression; Fig. 3E, Suppl. Fig 9C). Here, the primary sample generally showed slightly greater sensitivity. Although limited to two cases, these findings illustrate how tumor evolution – both genetic and phenotypic – could impact drug response, therefore highlighting the importance of drug sensitivity screening in newly acquired samples, rather than relying on archived models.

RNA expression correlates with *ex vivo* drug sensitivity of targeted compounds

Since genetic alterations alone could not reliably predict drug response, we explored correlations between pre-treatment gene expression and drug response across tumor types. Higher *BCL-2* expression was associated with venetoclax sensitivity across both cohorts, consistent with previous reports ($p < 0.012$; Fig. 4A; Suppl. Fig. 10A).[28] In addition, higher ALK expression correlated with sensitivity to the ALK inhibitors ceritinib and alectinib in the Máxima cohort (p =

0.002; p = 0.020, Fig. 4B, Suppl. Fig. 10C), though not in Curie, where lower concentrations were tested (Suppl. Fig. 2A-B, 10B-D). We did not find a significant correlation with ALK-expression and lorlatinib sensitivity (Máxima p=0.054; Curie p=0.39).

Genomic ALK alterations did not reliably predict sensitivity to ALK inhibition in neuroblastoma. Given the therapeutic relevance of ALK inhibitors, we explored whether baseline gene expression and master regulator (MR) activities were associated with response to alectinib, crizotinib, and lorlatinib across the two cohorts. These analyses focused on neuroblastoma samples. Single-gene analyses identified at least one overlapping gene associated with response to ALK inhibition in both cohorts: 11 for crizotinib, one for lorlatinib and two for alectinib (Suppl. Fig. 10E, 11A). However, we did not find a gene that was significantly associated to sensitivity to all ALK inhibitors in both cohorts. We excluded ceritinib from these analyses due to inconsistent results from the AUCnorm-based linear model.

Beyond individual genes, we examined pathway-level enrichments across both cohorts. Although both cohorts consist exclusively of neuroblastoma samples, the different culture conditions and experimental handling introduce substantial batch effects (Suppl. Fig. 11B). Pathway-level analyses help mitigate these technical differences by capturing coherent transcriptional programs that are more robust and reproducible than individual gene signals. Interferon *alpha* and *gamma*, and inflammatory responses were associated with response to crizotinib and lorlatinib in both cohorts (Fig 4C; Suppl. Fig. 11C). Conversely, pathways such as IL6 JAK STAT3 signaling and TNF alfa signaling displayed drug- and cohort-specific enrichment patterns.

Next, given that MRs orchestrate coordinated gene expression programs, we used the VIPER method[29] to explore if MR activity was associated to ALK inhibitor response in neuroblastoma. In each cohort, we identified MRs whose regulons were enriched within the AUC_{norm}-associated gene signatures for each compound. We found seven MRs (Fig. 4D) significantly associated with lorlatinib sensitivity in both the Máxima and Curie cohorts. Similarly, we identified 146 overlapping MRs for crizotinib (Supp. 12A) and 19 for alectinib (Supp. 12B) when comparing the two cohorts. Inferred activity of SMAD4 was associated with sensitivity to all three ALK inhibitors at Máxima, and a similar but non-significant pattern was observed in Curie (Suppl. Fig. 12C). These associations provide hypothesis-generating data on transcriptomic patterns that might be linked to ALK inhibitor response, which requires further validation.

Ex vivo drug sensitivity profiling complements molecular profiling in identifying clinically relevant drug hits

As molecular profiling alone does not identify enough drug candidates for all patients and has limited predictive power for treatment response,[7,11–13] we investigated identifying patient-specific drug options using *ex vivo* drug sensitivity profiling. To increase therapeutic precision whilst minimizing toxicity of drugs, we defined top responders per compound as samples whose AUC_{norm} and the IC50 both fell within the top 20% most responsive quantile (Fig. 5A-B). In the Máxima cohort (n = 35, excluding replicates of NB0277), a maximum of seven top responders per compound could be identified, while in the Curie cohort (n = 32), this was six. Not all compounds produced top hits, either due to insufficient drug efficacy (i.e., the IC50 was not achieved) or discrepancies between AUC_{norm} and IC50. Across both cohorts, 94% of patients (63 out of 67) had

at least one top hit and we found on average eleven functional top hits per patient (14.9 in Máxima, 6.8 in Curie) (Fig. 5C; Suppl. Fig. 13A-B). More importantly, we identified drug hits for 88% (11/13) of screens where no targetable alterations could be identified. For these samples, we identified eight PI3K /AKT and seven MAPK targeting compounds as top hits, which could be a potential pathway to further investigate. Furthermore, as a first-pass approximation of clinical achievability, we compared IC50 values with clinically achievable maximum doses (Cmax) for 134 compounds.[30] Among top hits with available Cmax values, 78% (391/501) had IC50s below Cmax, supporting the potential of functional top hits for clinical translation.

To demonstrate how *ex vivo* drug sensitivity profiling complements molecular profiling by expanding treatment options and refining drug selection, we compared functional top hits with molecular tumor board (MTB) reports including treatment recommendations, available for seven patients (Suppl. Tab. 4). We find overlapping compound targets and pathways in the MTB recommendations and functional top hits two patients. For two others we find overlapping compound targets in the MTB recommendations and functional top hits. *Ex vivo* drug sensitivity profiling broadened treatment options for six patients by identifying compounds targeting alternative pathways beyond MTB recommendations. To illustrate its role in refining drug selection, we highlight patient NB0277, that was screened in both institutes. We compared *ex vivo* drug sensitivities for compounds recommended by the MTB with those identified through *ex vivo* drug sensitivity profiling (Fig. 5D; Fig. 12C-D). The MTB recommended ALK inhibitors based on ALK amplification, and mTOR inhibitors (everolimus, combined with topoisomerase inhibitor topotecan) due to MYCN amplification. Although *ex vivo* drug sensitivity profiling did not identify mTOR inhibitors as top hits, two ALK inhibitors (alectinib and lorlatinib) were identified as drug

top hits (Fig. 5D). Next to this, IC50 values of ceritinib were below Cmax in both institutes. Together, these results strengthen ALK inhibition as a promising therapeutic avenue. *Ex vivo* drug sensitivity further broadened treatment options by identifying additional drug classes, including BCL-2 inhibitors venetoclax and navitoclax, MEK inhibitors trametinib and pimasertib, and EGFR inhibitors afatinib and erlotinib in the Máxima (Fig. 5D; Suppl. Fig. 13C), and topoisomerase inhibitor mitoxantrone and cisplatin in Curie (Suppl. Fig. 13D). The differences between the institutes reflect the distinct cohort compositions, where different tumor types are included. These functional top hits highlight expanded therapeutic opportunities compared to genomic profiling alone. In this illustrative case, ALK inhibition remains the most promising strategy as it is suggested both based on the molecular and drug sensitivity profiles. Taken together, these findings demonstrate that *ex vivo* drug sensitivity profiling could be used to complement and extend suggestions for molecularly guided treatment choices and identify additional therapeutic options.

Discussion

Molecular profiling alone often fails to predict effective therapies in high-risk pediatric tumors.[11,13] This has been confirmed in recent large-scale pediatric precision oncology programs including ITHER,[7] INFORM,[6] MAPPYACTS,[4] and ZERO.[8,10,12] These studies showed that only a small subset of patients with recurrent or high-risk tumors harbored high-evidence actionable mutations. Furthermore, a minority of patients with lower evidence level targets received matched therapies (in part because of absence of clinical trials) and overall derived relatively low clinical benefit of the suggested treatments. The need for improved prediction of drug response is particularly pressing in pediatric oncology, where in addition to the underlying cancer

complexity, the rarity and diversity of tumor types limits cohort sizes and hamper biomarker discovery. In this context, we conducted a proof-of-concept study to assess whether rapid *ex vivo* drug screening can complement genomic and transcriptomic profiling across pediatric solid tumors. We successfully tested drug sensitivity in 69 *ex vivo* cultures from previously established PDX samples and observed consistent trends in drug sensitivity across cohorts. *Ex vivo* responses were achieved within 14 days after receiving the PDX samples. Our results show that *ex vivo* drug sensitivity profiling can complement molecular profiling by providing drug hits for a majority of samples. These findings support the potential relevance of *ex vivo* drug sensitivity profiling alongside genomics and transcriptomics in an integrated diagnostic platform to facilitate clinical decision-making. Below, we evaluate the technical feasibility, success rate, clinical relevance of the screens, and the potential added value of *ex vivo* drug sensitivity profiling in a precision oncology setting.

We successfully performed 69 drug screens (82% success rate), achieving *ex vivo* drug sensitivity profiles within 14 days, and observed consistent trends in drug sensitivity across institutes. All results presented in this study were derived from *ex vivo* cultures of previously established PDXs. The dissociated PDX samples provide comparable material to that of patient resections,[31] but higher biomass than samples obtained directly from patient (fine needle) biopsies. This enabled us to test larger drug libraries and perform reproducibility screening. However, using PDX-expanded material comes with limitations. First, the high success rate is likely explained by a selection bias toward more aggressive tumors, as also reported in pediatric sarcomas.[32] For comparison, the INFORM study, using fresh patient samples, reported sufficient viable tissue in 67% of cases, of which 78% passed internal quality control.[19] Second, the

establishment and expansion of PDX models typically require several months,[32–34] often exceeding the time to progression described in INFORM registry.[6] However, once PDX-expanded tumors were received and cultured *ex vivo*, drug screens and data processing were completed within 14 days, which is aligned with the timeline of molecular profiling, and comparable with the *ex vivo* drug screening timeframe reported in INFORM.[6,7,19] For clinical translation, we are conducting rapid screening of fresh patient samples, without an intervening PDX model, to achieve turn-around times compatible with clinical decision making. To improve success rates for these low-biomass samples, we recommend using round-bottom plates (requiring ~500 instead of 5,000-20,000 cells per well) and tumor-type guided compound prioritization.

Despite differences in drug screening protocols at Máxima and Curie, we observed high correlation and consistent top-effective compounds across overlapping models. This demonstrates the robustness of *ex vivo* drug screening across institutes. Nevertheless, differences in drug response may reflect protocol variations between Máxima and Curie: *ex vivo* expansion time (7 days versus direct seeding), cell densities (5,000 versus 20,000), dose ranges (Suppl. Fig. 2) and drug libraries (e.g., different compound batches). In addition, different passages of PDX models and concomitant clonal selection, could influence *ex vivo* drug response. Growth rate was assessed only in Máxima, serving as an indicator of sample quality, with growth rates below 100% reflecting spontaneous cell death in the absence of treatment. Growth rate correlated with response to cytotoxic and cell-cycle targeting agents, consistent with known mechanisms.[35] As proliferation rates of *ex vivo* cultures are typically higher than patient tumors, anti-tumor effects of mitotic inhibitors might be overestimated.[36] To improve comparability across models with variable growth dynamics, we recommend including growth rate as a

standardized quality control metric.[35] Improving cross-institute comparison could result in large-scale cohorts, which are valuable for rare diseases, as exemplified by initiatives such as COMPASS and the Society for Functional Precision Medicine (ERAPERMED2018-121).[13] To further test cross-site variability we are performing cross-site benchmarking experiments within the COMPASS consortium. To enhance the potential for wider clinical implementation, we therefore propose a harmonized protocol: 384-round bottom plates with standardized input (e.g. 500 cells per well), standardized quality control metrics (such as growth rate), agreed dose-ranges and compound libraries prioritized per tumor type, standardized timeframes of *ex vivo* expansion, and cross-site control samples.

Through collaboration between the two institutes, we increased sample sizes, enabling the exploration of tumor type specific sensitivities, including tumor types that are difficult to model *in vitro*, such as osteosarcoma.[23] However, the heterogeneity and small sample sizes for several tumor types does limit the identification of robust subtype-specific drug responses and our findings must therefore be considered. Data correlating *ex vivo* sensitivity with patient response is rare in pediatric cancers yet is essential to validate drug response patterns. As an example, while Ewing sarcoma samples in our study showed sensitivity to PARP inhibitor *ex vivo*, consistent with other *in vitro* and *in vivo* studies,[37,38] clinical trials of PARP inhibition in Ewing have not shown durable benefit.[39–41] By contrast, INFORM reported parallels between *ex vivo* drug sensitivities and clinical courses in selected cases, such as complete resistance to the multidrug RIST regimen in relapsed Ewing sarcoma.[13,19] Validating clinical outcomes in large pediatric cohorts remains a critical challenge for functional precision medicine programs.

Beyond tumor-type-specific associations, we examined associations with drug response and molecular profiling across the full cohorts. Here, pan-cancer analyses can be confounded by tumor-type bias. While MYCN and ALK alterations appeared linked to drug sensitivity in pan-cancer, this link disappeared when restricted to neuroblastoma, indicating they were confounded by tumor-type sensitivity rather than the alteration. To address this, we explored ALK inhibitor response and transcriptomic changes within neuroblastoma alone. We found associations with ALK expression and response to selected ALK inhibitors, consistent with previous findings.[42] However, single genes and pathways did not result in consistent associations across all ALK inhibitors in both institutes. We therefore used master regulator analysis, which integrates the collective behavior of target gene networks which can reveal conserved regulatory programs that may be critical for modulating drug response.[29] Although only significant in Máxima, higher baseline SMAD4 activity was associated with sensitivity to all three ALK inhibitors in both institutes. SMAD4 has tumor-suppressive roles in neuroblastoma and can be functionally inactivated by ALK-mediated phosphorylation.[43,44] Tumors with higher baseline SMAD4 activity could be more sensitive to ALK inhibition, as blocking ALK could restore SMAD4-dependent tumor suppression.[43,44] These results provide hypothesis-generating data and will require follow-up studies consisting of functional assays and *in vivo* PDX validations. While the potential of transcriptomics should be further validated in patients, our results suggest that relying solely on genomic status for trial eligibility may exclude patients who could benefit from ALK inhibition based on functional or transcriptomic profiles.

To assess potential predictive markers of drug sensitivity, we compared different approaches commonly used in a precision medicine context: genetic biomarkers, transcriptional

biomarkers, and *ex vivo* drug screening. No targetable genetic alterations could be identified in 13 out of 69 screens, underscoring a common limitation in pediatric precision oncology.[4,6] Consistent with prior studies, when targetable alterations were detected, they did not consistently predict *ex vivo* drug response.[13] For example, CDK4 amplification did not associate with sensitivity to cell cycle inhibitors, in line with prior reports.[12,45] At the individual patient level, functional profiling may add clinical value by complementing molecular profiling. Using a selective outlier approach, we identified drug hits for 94% of samples, including 12 out of 13 cases where no targetable alteration was identified. These findings demonstrate that *ex vivo* drug sensitivity profiling can expand therapeutic suggestions, especially in patients whose tumors lack targetable alterations. When an alteration is found, *ex vivo* drug sensitivity profiling can be used to refine the choice of compound. We used Cmax to estimate clinical achievability of *ex vivo* determined IC50 values, a strategy previously applied in *in vitro* drug screening.[10] While useful as a first-pass filter, Cmax-IC50 comparisons do not capture *in vivo* pharmacokinetic and pharmacodynamic processes.[30,46] For example, plasma protein binding, drug lipophilicity and tissue distribution can strongly influence free drug exposure at the tumor site and should be integrated in future *in vitro* work.[47,48] Although this proof-of-concept study only included technical reproducibility as validation, biological validation will be pursued via matched *in vivo* testing. The ITCC-P4 consortium provides a platform for testing *in vitro*-identified drugs across a broad range of *in vivo* pediatric tumor models and is currently comparing the therapeutic efficacy of standard of care compounds with new investigational compounds or targeted therapies in this panel. Sixty of the models used here have matched PDX counterparts in ITCC-P4, enabling future validation of *ex vivo* hits *in vivo*. As an example, standard of care compounds for neuroblastoma

will include etoposide and topotecan and investigational drugs such as idasanutlin, cobimetinib, various ALK inhibitors, prexasertib and copanlisib.

Taken together, our study provides a proof-of-concept for the feasibility of rapid *ex vivo* drug screening in pediatric precision oncology. Currently, this method is being expanded to include fresh patient samples. Our data support the future integration of functional profiling into a next-generation diagnostic platform that combines *ex vivo* drug sensitivity profiles with genetic and transcriptomic data to predict drug response.

Methods

Tissue Processing and Drug Screening Protocols

Ex vivo short-term drug sensitivity screening was performed at two centers, Princess Máxima Center (Máxima) and Curie Institute (Curie), using fresh patient-derived xenograft (PDX) tumor material. This method aimed to assess *ex vivo* drug sensitivity profiling within a clinically relevant timeframe and to complement molecular profiling in pediatric precision oncology.

PDX establishment

PDX establishment and characterization was conducted in the ITCC-P4 consortium as previously reported.[11,49] 37 PDX models in the Máxima and 32 PDX models in Curie were selected and successfully screened *ex vivo*.

In short, PDXs worked up in the Máxima were established by EPO, Charles River and Xentech, where informed consent was obtained from patients or parents/caregivers prior to the collection of biological samples in accordance with the study protocol approved by the Ethics Board of the

Medical Faculty of the University of Heidelberg. For each patient, fresh tumor material (surgical resection or biopsy), a constitutional (germline) sample and clinical information was collected. Solid tumors were transferred in cell culture medium and transplanted subcutaneously in NSG (NOD.Cg-Prkdcscid IL2rgtm1Wjl/SzJ), Swiss Nude (Crl:NU(Ico)-Foxn1nu) or CB17 SCID (CB17/Icr-Prkdcscid/IcrIcoCrl) immunodeficient mice.

At Institut Curie, PDXs were established from tumor biopsies obtained at diagnosis or at relapse, as described previously,[11] following informed consent of parents or guardians. Experimental procedures were approved by the ethics committee of the Curie Institute CEEA-IC #118 (Authorization APAFIS#11206-2017090816044613-v2) in compliance with international guidelines. The establishment of PDX models received approval by the Institut Curie institutional review board OBS170323 CPP ref 3272; n° 2015-A00464-45). In brief, tumor samples were engrafted subcutaneously in immunocompromised mice.

Upon successful establishment (> P2) and upon reaching ethical size, PDX tumors were cryopreserved for banking and further analyses. All PDXs from the Máxima, and 24 PDXs from Curie were integrated within the ITCC P4 consortium. For these models, all human and corresponding PDX samples, along with associated clinical, and molecular data, were anonymized and labeled using a barcoding system. This system encoded information about the original source, tumor entity, tumor event, sample type, and data type. Barcodes were automatically generated upon sample and patient data registration in the R2 online platform (r2-itccp4. amc.nl). For models not included in the ITCC P4 consortium, institutional anonymization was used (models IC-pPDX-### and models HSDJ_###).

PDX molecular profiling

Comprehensive molecular profiling was conducted on PDX tumor samples and whenever possible on patient tumor and germline control. DNA and RNA were extracted from samples using standardized procedures.[4,7] For low coverage whole genome (lcWGS)/whole exome sequencing (WES) library preparation was performed using standardized procedures,[9] followed by capture using the Agilent SureSelect Clinical Research Exome V2 Kit, and sequenced using the Illumina R technologies. For DNA methylation array profiling, Methylation450K and MethylationEPIC BeadChip arrays (Illumina) were used. RNAseq Library construction was performed following the TruSeq Stranded mRNA LS protocol (Illumina, San Diego, CA). Sequencing was performed on Illumina sequencing machines: NextSeq 500 (150 nt paired-end) and NovaSeq (100 nt paired-end).

Calling of genetic events

NGS and methylation data was manually curated following visualization on the R2: Genomics Analysis and Visualization platform (http://r2.amc.nl). Data was used for calling of CNVs, SNVs and SVs/fusions predicted to be actionable, as described previously.[4,7] For ALK, MYCN, TERT, and CDK4 high level genomic amplification were called as amplifications (copy number >log2). ALK alterations were also called in case of an activating mutation within the tyrosine kinase domain. Alterations in genes with suppressor gene function (SMARCA4, SMARCB1, NF1, ATM, PALB2, CHEK2, BRCA2, PTCH1 and PTEN) were considered in case of homozygous deletion, or loss of heterozygosity (LOH) in combination with an inactivating mutation.[50] Mutations in ATRX were called in case of homozygous inactivating events or deletion, or the combination of LOH, in-frame

fusions, inactivating mutations, or hotspot mutations. Clinically relevant STAG2 was called in case of inactivating mutations.[51] CDKN2A/CDKN2B alterations were considered in case of homozygous deletions. TP53 mutations were called when a deletion occurred together with an inactivating (frameshift or SNV) mutation (and heterozygous was annotated but not used in analysis, unless stated otherwise). HRAS was called in case of activating mutations (hotspot regions).

Determining mice contamination in *ex vivo* short-term screen samples

Mouse contamination in screened samples was determined either based on DNA (27 cases, at Máxima) or based on RNA analyses (33, at Curie).

Prior to real-time quantitative PCR (RT-qPCR), genomic DNA extraction was carried out for all tested samples. Following DNA extraction and measurements, RT-qPCR was performed using the CFX384 Touch Real-Time PCR Detection System (BioRad). To measure the amount of either human or murine genomic DNA concentrations, two separate Go-Taq® qPCR-based (LOT: 0000602761) master mixes (MM) were prepared, one to probe human DNA and one to probe murine DNA. For each reaction, 4,6 µL H2O, 10 µL Go-Taq® qPCR MM, either 0,2 µL forward human primer (REF: 2378847) or 0,2 forward murine primer (REF: 2378849) and 0,2 µL reverse human-murine primer (REF: 2378848), totaling 15 µL of MM, was added to 5 µL of 1 ng/ µL of isolated DNA, together with positive and negative controls. The positive human and murine controls were added to the plate in de-escalating human-murine ratios to more accurately determine human-murine ratios in the PDX samples. The ratios were set as follows: H100:0M, H99:1M, H95:5M, H80:20M, H20:80M, H0:100M. Cycling conditions included an initial denaturation of 5 minutes at 95 °C, followed by 40 cycles of 45 seconds at 95 °C and 30 seconds

at 60 °C, ending on an extension of 90 seconds on 72 °C. Melting curve analysis was performed to assess specificity of amplification and Cq values. Human and murine control ratios were used to determine the true human-murine ratios in the PDX models.

RNAseq fastq files were processed by Institut Curie RNAseq pipeline version 4.1.0 with xgensort tool (https://gitlab.com/genomeinformatics/xengsort) to select reads coming from the human tumor, while filtering out mouse reads.

Tissue dissociation, cell culture and cell seeding

At both centers, tumor tissues were mechanically and enzymatically dissociated to obtain single-cell suspension for *ex vivo* drug screening in flat bottom 384-well plates. While core principles were shared, protocol details regarding enzyme combinations, media composition, and expansion time before seeding differed between the Máxima and Institut Curie.

At the Máxima, tumor tissues were first mechanically dissociated using sterile scalpels, followed by a two-step enzymatic digestion. Initially, tissues were transferred to Liberase DL (Sigma Aldrich, cat no. 5466202001) at a 1:43 dilution in tumor stem media (TSM) base, as reported before.[19,52] Tumor pieces are digested at 37°C for 30 minutes, with intermittent swirling. Supernatant was collected and filtered through a pre-washed 70 µm strainer. On the remaining tumor pieces, a second digestion step was performed in a digestion buffer of Liberase TM (Sigma Aldrich, cat no. 5401119001) at a 1:43 dilution in TSM base for another 30 minutes at 37°C, with intermittent swirling. Following each harvest, cells were centrifuged at 300 g for 5 minutes. Red blood cells were lysed using a red blood cell lysis buffer, with a maximum of 4 minutes incubation at room temperature. Post-lysis, cells were suspended in TSM complete [19,52] and counted using

trypan blue. Tumor cells were cultured for 7 days before drug screening in TSM complete, at 37°C and 5% CO2. 40 µL of cells, aiming for 5,000 cells/well, are plated in a flat bottom 384-well tissue culture treated microplate (#3764, Corning, NY) using a multidrop combi reagent dispenser (Thermo Scientific). Total DNA was isolated and processed at the time of plating.

At Institut Curie, freshly collected PDX tumors were first dissociated as described previously [17]. After mechanical dissociation using sterile scalpels, enzymatic dissociation with trypsin (10 mg/ml) and type II collagenase (275 U/mg, Worthington Biochemical) was performed. The tube was then placed in a warm 37°C water bath for 60 minutes. Dissociation was stopped by adding Soybean Trypsin Inhibitor (10 mg/ml, Sigma). Deoxyribonuclease I (2 mg/ml, Sigma) and magnesium chloride (1 M) were added in equal amounts. The tumor suspension was filtered through a 40 µm cell strainer and then centrifuged at 500g for 5 minutes. The supernatant was discarded, and cell pellet was resuspended in PBS-minus/10% FBS for cell counting. The suspension was then re-centrifuged and resuspended in serum-free stem-cell (SC) medium, which contained Dulbecco's Modified Eagle Medium/Nutrient Mixture F-12 (DMEM/F12, Gibco) supplemented with 40 ng/ml basic fibroblast growth factor (bFGF), 20 ng/ml epidermal growth factor (EGF), 1× B27 supplement (Gibco) and 500 U/ml of penicillin/streptomycin. Dissociated cells were directly seeded in flat bottom 384-well plates for drug screening without any pre-culture amplification phase. 25 µl of cells (20,000 cells/well) prepared in serum-free stem cell (SC) medium was dispensed into each well using a MultiDrop Combi (Thermo Fisher).

High-throughput compound screening

At both centers, high-throughput compound screening was performed to determine drug sensitivity profiles in *ex vivo* cultured PDX-derived tumor cells. Common principles included the use of flat bottom 384-well plates, incubation with compound libraries across multiple concentrations, and luminescence-based viability assays after 72h. Clinically relevant compounds were added using acoustic dispensing systems and screening was conducted in technical duplicates. Differences between the two sites involved compound library composition, dosing schemes, cell numbers, and assay reagents.

In Máxima, screening was performed in two versions of its internal Princess Máxima Center library - version L13 and L14 -, which contains 224 and 225 drugs respectively. These libraries include compounds that are FDA approved, or in (pre-)clinical evaluation (Suppl. Tab. 1). For samples with limited biomass, a 134-compound clinical priority subset was applied. Most of the compounds from the libraries are dissolved in dimethylsulfoxide (DMSO) and stored at room temperature under nitrogen atmosphere. Five (metformin, perifosine, carboplatin oxaliplatin and copanlisib) drugs are dissolved in MQ and one (cisplatin) is dissolved in a saline solution, which are stored at -20 °C. Before the high-throughput screening, the 384-well plates (Well Low Dead Volume Source Microplates, Labcyte) containing the dissolved drugs are shaken (30 minutes at rt) and centrifuged (2.30 minutes at 1500 rpm). Subsequently, the plates are surveyed with the Echo 550 dispenser to determine whether the amount of solution in the wells is sufficient to start the screen (minimal 2.5 µl) and the DMSO percentage is >80%.

In Institut Curie, the Compass03 oncology collection, covering a total of 74 oncology drugs (mainly FDA/EMA approved) and control drugs designed for COMPASS study, was used (Suppl.

Tab. 2) [19,53]. All compounds were obtained from commercial compound vendors. The compounds were dissolved in 100% DMSO or MQ.

In Máxima, high-throughput drug screens were conducted in duplicate in collaboration with the high-throughput screening facility of the Princess Máxima Center. Cells are cultured for 24h under standard culturing conditions (5% CO_2, 37 °C). Next, the Cell Titer Glo 3D (CTG3D, Promega, USA, G9683) cell viability assay is performed for the t = 0 microplate using the supplier's protocol by measuring luminescence. Units of luminescence signal generated by a thermo-stable luciferase are proportional to the amount of ATP presented in viable cells. Furthermore, the drugs are added to tissue culture microplates and the library using the high-throughput screening facility (https://research.prinsesMáximacentrum.nl/en/core-facilities/high-throughput-screening). Using the Echo 550 dispenser, 100 nL of the drugs (in DMSO or MQ, at different concentrations) are added to the wells containing the cells, to yield final concentrations of 0,1 nM, 1 nM, 10 nM, 100 nM, 1 µM and 10 µM (0.25% DMSO or MQ). Cells treated with only DMSO are used as negative controls, whereas cells treated with staurosporine (final concentration of 10 µM) are used as positive controls. The cells are incubated with the compounds for 72h at standard culturing conditions. Next, after 72h of incubation, the CTG3D assay is performed for the microplates. Growth rates of the DMSO-treated cells during the screen are determined by dividing the CTG3D signal of the DMSO controls at day 3 by the signal at t0 (cell growth). In addition, to assess culture quality, microscopic inspection and imaging are performed at both timepoints.

At Institut Curie, 384-well plates with cells were also incubated for 24h at 37°C. Next, the compounds were dispensed using an acoustic liquid handling device, Echo 550 (Beckman Coulter)

at FIMM High Throughput Biomedicine unit (University of Helsinki, Finland; https://www.helsinki.fi/en/infrastructures/drug-discovery-chemical-biology-and-screening/infrastructures/fimm-high-throughput-biomedicine-unit) in three 384-well microplates (Corning - 3764). All drugs were plated in duplicates in five different concentrations in 10-fold dilutions covering a 10,000-fold concentration range (e.g. 1- 10,000 nM) mostly encompassing the achievable plasma concentrations in pediatric patients [19,53]. The cells are incubated with the compounds for 72h at standard culturing conditions. Drug effects on cell viability were measured using the CellTiter-Glo 2.0 Luminescent Cell Viability Assay (Promega). The reagent was equilibrated to RT for 30 minutes prior to use. A volume of 25 µl per well of CTG reagent was added in each well, mixed for 2 minutes at 300 rpm on an orbital shaker (Titramax 100). Plates were further incubated for 10 minutes at RT to stabilize luminescence signals. Luminescence was recorded using a CLARIOStar (BMG Labtech) (gain = 3600) using top measurement.

Data processing

In all cases, following high-throughput drug screening, the data is normalized to the 0.25% DMSO-treated cells (defined as 100% viability) and the empty controls (0% viability). Dose-response curves were estimated by a 5 parameters log-logistic model using the R package *drc* (version 3.0.1 with R 4.3.1; [54] From these fitted models several values were estimated: the concentrations of the drug needed to achieve a 50% reduction in cell viability (IC50), the definite integral of the curve (area under the curve, AUC). AUCs were normalized by the range of concentration for each compound as AUC_{norm} score to compare the two cohorts. Quality of the screens was approved

after assessment of the cell growth, the negative, positive, and empty controls, and the amount of variability between the duplicates. After processing, in the Máxima, a standard quality check is performed by high-throughput screening facility as well as a manual check per compound.

AUC_{norm} are used when analyzing within one cohort to define and compare drug sensitivities, as IC50s are not reached for ineffective compounds. When comparing two different cohorts with different dose ranges, the IC50 is used to compare drug sensitivities. In rare cases, normalized viability exceeded 100% at non-effective concentrations, resulting in an AUC_{norm} slightly above 100. This was retained to avoid artificial truncation of the curve and reflects occasional biological or technical variability. NB0277 was received three times due to a sample mislabeling. Only the first received sample was included in all analyses, except for the reproducibility testing (Fig. 1E) and growth-rate correlations (Fig. 3C), where the other two samples are also included.

Tumor type compound specificity

To assess the specificity of compound responses across tumor types, an analysis of variance (ANOVA) model was employed, between AUC_{norm} and tumor type as covariate. Compounds yielding a p-value ≤ 0.05 were considered to exhibit statistically significant differential responses among tumor types. To further investigate tumor-type-specific efficacy, t-tests were conducted comparing each tumor type against the pooled set of all other types. This analysis aimed to identify compounds with significantly higher or lower AUC_{norm} values in specific tumor types relative to others.

Identifying transcriptomic signatures linked to drug sensitivity

To identify genes whose expression correlates with AUC_{norm} differential gene expression analysis was performed using DESeq2 (v 1.44.0)[55] in R version 4.4.1. Raw count data were filtered to remove lowly expressed genes, retaining only those with a minimum expression threshold in multiple samples. Counts were normalized using the median-of-ratios method to account for differences in sequencing depth. Both drug response (AUC_{norm}) and gene expression were modeled as a continuous variable (no dichotomization), using a generalized linear model (GLM) of the form:

$$Expression \sim AUC_{norm}$$

where AUC_{norm} represents the drug sensitivity score for each sample. Wald tests were used to assess statistical significance, and Benjamini–Hochberg (BH) correction was applied to control for false discovery rate (FDR). Genes with adjusted p-values (padj) < 0.05 were considered significant. We excluded ceritinib from the analysis due to inconsistent results from the AUC_{norm}-based linear model.

Pathway enrichment analysis was performed using Gene Set Enrichment Analysis (GSEA) with the fgsea (v 1.30.0)[56] package in R. Genes were ranked based on Wald test statistics from DESeq2, preserving the direction of association with AUC_{norm}. Hallmark gene sets were obtained from the Molecular Signatures Database (MSigDB) [57] using the msigdbr (v 7.5.1) [58] package in R, for enrichment analysis. The fgsea algorithm was run with 1,000 permutations, using a minimum gene set size of 15 and a maximum of 500 to exclude nonspecific pathways. Pathways with adjusted pvalue < 0.05 were considered significantly enriched.

Master regulator (MR) analysis was performed using VIPER (v 1.38.0; [59]) to infer the activity of transcription factors (TFs) associated with drug sensitivity in neuroblastoma. Two complementary approaches were employed: msVIPER, which identifies MRs at the cohort level by integrating gene-level differential expression data, and VIPER, which infers MR activity at the individual sample level. To identify TFs driving AUC_{norm}-associated transcriptional changes, the *msviper()* function was applied to the gene signature defined as described in the "Identifying transcriptomic signatures linked to drug sensitivity" section above, using a neuroblastoma-specific regulatory network constructed from ARACNe-inferred[60,61] TF-target interactions derived from the SEQC dataset of 498 bulk RNA-seq neuroblastoma samples. [62] Enrichment significance was assessed using adaptive-weighted Kolmogorov–Smirnov statistics with 1000 permutations. All analyses were conducted in R version 4.4.1 using VIPER with a neuroblastoma-specific regulon derived from publicly available expression datasets, applying default parameters unless otherwise specified.

Data access statement

The data presented in this study are available via the R2 Genomics Analysis and Visualization Platform (https://r2.amc.nl).

Acknowledgements

We thank all patients and their parents for providing samples that made this research possible. We appreciate the support given by the following core facilities: High Throughput Screening Facility in the Princess Máxima Center and BioPhenics High-Content Screening Laboratory in the Curie institute, and FIMM High Throughput Biomedicine Core unit (supported by EU OPENSCREEN and BioCenter Finland). We would like to thank our collaborators of the ITCCP4 consortium for sharing their knowledge and resources. The part of this work that is performed in the Máxima was supported within the framework of the IMI2 ITCC-P4 program (grant agreement no. 116064). In addition, the molecular characterization of some PDX models and the IRCCS—Istituto Ortopedico Rizzoli, Experimental Oncology Laboratory, Bologna, Italy, (Katia Scotlandi), was supported by the IMI2 ITCC-P4 program (grant agreement no. 116064). We acknowledge the role of the Italian Alliance against Cancer for coordinating the participation in the ITCC-P4 project. Ellora Chua is supported by the EuReCa international PhD program granted to Institut Curie. At Institut Curie, this study was supported by the Ligue contre le Cancer (Projet de Recherche Enfants, Adolescents et Cancer de la Ligue Contre le Cancer), the Annenberg Foundation, the Association Hubert Gouin Enfance et Cancer, Imagine for Margo, the Fondation ARC pour la Recherche contre le Cancer (ARC), Agence Nationale de la Recherche (ANR) and the EraPerMed2018 funding call. Establishment of some PDX models was performed under the MAPPYACTS protocol (clinicaltrial.gov: NCT02613962). Part of this work was supported by the

Aamu Foundation and the Cancer Foundation. The FIMM High Throughput Biomedicine unit is supported by the University of Helsinki and Biocenter Finland, Finnish Cultural Foundation, and Väre Foundation (VP). Figure 1A was created in BioRender (Molenaar, J., 2025; https://BioRender.com/002la1z).

Author contributions

Marlinde. C. Schoonbeek: conceptualization, data curation, analyses, investigation, methodology, writing- origional draft, visualisation, project administration. Pierre Gestraud: data curation, analyses, visualisation, writing – origional draft. Lindy Vernooij: investigation, project administration. Arjan Boltjes: analyses, visualisation. Vicky Amo-Addae: methodology, recources (Máxima library). Marloes van Luik: analyses, visualisation. Elaine Del Nery: methodology, investigation. Angela Bellini: investigation, methodology. Ellora Chua: data curation, analyses, visualisation, origional draft. Sarah Swaak: investigation. Eleonora Looze: investigation, writing – review & editing. Vilja M. Pietiäinen, Laura L. Turunen, Jani S. Saarela: methodology, resources (COMPASS drug library). Julia Schueler, Emilie Indersie, Dennis Gürgen, Katia Scotlandi, Angelika Eggert, Rachida Bouarich, Franck Bourdeaut, Sakina Zaidi, Didier Surdez, Ángel M. Carcaboso, Birgit Geoerger: methodology, recources (PDX models). Elnaz Saberi-Ansari: data curation and analyses. Yasmine Iddir and Alexandra Saint-Charles: project administration. Florence Cavalli: supervision, writing – review & editing. Apurva Gopisetty and Eva Maria Rief: project administration (ITCCP4). Hubert N Caron, Lou Stancato, Gilles Vassal, Stefan Pfister: supervision (ITCCP4), writing – review & editing. Jan Koster: resources (R2 platform). Selma Eising: methodology, supervision, conceptualization, writing – review & editing. Sander R. van Hooff, Marlinde L. van den Boogaard: supervision, writing – review &

editing. Gudrun Schleiermacher, J.J. Molenaar: conceptualization, supervision, writing – review & editing.

Conflict of interest statement

Gudrun Schleiermacher receives research funding from Roche, BMS, Pfizer and MSD. The other authors declare no competing interests related to this study.

Key words

Precision oncology, high-throughput drug screening, pediatric oncology, precision medicine, high-risk solid tumors, neuroblastoma, transcriptomic biomarkers, drug repurposing

References

1. Steliarova-Foucher, E. *et al.* Changing geographical patterns and trends in cancer incidence in children and adolescents in Europe, 1991–2010 (Automated Childhood Cancer Information System): a population-based study. *Lancet Oncol* **19**, 1159–1169 (2018).
2. Pfister, S. M. *et al.* A Summary of the Inaugural WHO Classification of Pediatric Tumors: Transitioning from the Optical into the Molecular Era. *Cancer Discov* **12**, 331–355 (2022).
3. Burdach, S., Westhoff, M.-A., Steinhauser, M. F. & Debatin, K.-M. Precision Medicine in Pediatric Oncology. *Mol Cell Pediatr* **5**, (2018).
4. Berlanga, P. *et al.* The European MAPPYACTS trial: precision medicine program in pediatric and adolescent patients with recurrent malignancies. *Cancer Discov* **12**, 1266–1281 (2022).
5. Heipertz, A. E. *et al.* Outcome of Children and Adolescents With Relapsed/Refractory/Progressive Malignancies Treated With Molecularly Informed Targeted Drugs in the Pediatric Precision Oncology Registry INFORM. *JCO Precis Oncol* **7**, e2300015 (2023).
6. van Tilburg, C. M. *et al.* The Pediatric Precision Oncology INFORM Registry: Clinical Outcome and Benefit for Patients with Very High-Evidence Targets. *Cancer Discov* **11**, 2764–2779 (2021).
7. Langenberg, K. P. S. *et al.* Implementation of paediatric precision oncology into clinical practice: The Individualized Therapies for Children with cancer program 'iTHER'. *Eur J Cancer* **175**, 311–325 (2022).
8. Wong, M. *et al.* Whole genome, transcriptome and methylome profiling enhances actionable target discovery in high-risk pediatric cancer. *Nat Med* **26**, 1742–1753 (2020).

9. Bayat, B., Raj, R., Graf, A., Vereecken, H. & Montzka, C. Comprehensive accuracy assessment of long-term geostationary SEVIRI-MSG evapotranspiration estimates across Europe. *Remote Sens Environ* **301**, 113875 (2024).
10. Lau, L. M. *et al.* In vitro and in vivo drug screens of tumor cells identify novel therapies for high-risk child cancer. *EMBO Mol Med* **14**, e14608 (2022).
11. Marquart, J., Chen, E. Y. & Prasad, V. Estimation of the percentage of US patients with cancer who benefit from genome-driven oncology. *JAMA Oncol* **4**, 1093–1098 (2018).
12. Mayoh, C. *et al.* High-Throughput Drug Screening of Primary Tumor Cells Identifies Therapeutic Strategies for Treating Children with High-Risk Cancer. *Cancer Res* **83**, 2716–2732 (2023).
13. Letai, A., Bhola, P. & Welm, A. L. Functional precision oncology: testing tumors with drugs to identify vulnerabilities and novel combinations. *Cancer Cell* **40**, 26–35 (2022).
14. Letai, A. Functional precision cancer medicine-moving beyond pure genomics. *Nat Med* **23**, 1028–1035 (2017).
15. Marques Da Costa, M. E. *et al.* A biobank of pediatric patient-derived-xenograft models in cancer precision medicine trial MAPPYACTS for relapsed and refractory tumors. *Commun Biol* **6**, 1–15 (2023).
16. Pauli, C. *et al.* Personalized in vitro and in vivo cancer models to guide precision medicine. *Cancer Discov* **7**, 462–477 (2017).
17. Stewart, E. *et al.* Orthotopic patient-derived xenografts of paediatric solid tumours. *Nature* **549**, 96–100 (2017).
18. Langenberg, K. P. S. *et al.* Exploring high-throughput drug sensitivity testing in neuroblastoma cell lines and patient-derived tumor organoids in the era of precision medicine. *Eur J Cancer* **218**, (2025).
19. Peterziel, H. *et al.* Drug sensitivity profiling of 3D tumor tissue cultures in the pediatric precision oncology program INFORM. *NPJ Precis Oncol* **6**, (2022).
20. Acanda De La Rocha, A. M. *et al.* Feasibility of functional precision medicine for guiding treatment of relapsed or refractory pediatric cancers. *Nat Med* 1–11 (2024) doi:10.1038/s41591-024-02999-2.
21. Lee, J. K. *et al.* Pharmacogenomic landscape of patient-derived tumor cells informs precision oncology therapy. *Nat Genet* **50**, 1399–1411 (2018).
22. Sun, H. *et al.* Comprehensive characterization of 536 patient-derived xenograft models prioritizes candidates for targeted treatment. *Nat Commun* **12**, 5086 (2021).
23. Corre, I., Verrecchia, F., Crenn, V., Redini, F. & Trichet, V. The osteosarcoma microenvironment: a complex but targetable ecosystem. *Cells* **9**, 976 (2020).
24. Skalniak, L. *et al.* Prolonged idasanutlin (Rg7388) treatment leads to the generation of p53-mutated cells. *Cancers (Basel)* **10**, 1–17 (2018).
25. Lehmann, C., Friess, T., Birzele, F., Kiialainen, A. & Dangl, M. Superior anti-tumor activity of the MDM2 antagonist idasanutlin and the Bcl-2 inhibitor venetoclax in p53 wild-type acute myeloid leukemia models. *J Hematol Oncol* **9**, 1–13 (2016).
26. Gouda, M. A. & Thein, K. Z. Selinexor: Changing the paradigm in patients with TP53 wild-type endometrial cancer? *Med* **4**, 752–754 (2023).
27. Montesinos, P. *et al.* MIRROS: A randomized, placebo-controlled, Phase III trial of cytarabine ± idasanutlin in relapsed or refractory acute myeloid leukemia. *Future Oncology* **16**, 807–815 (2020).

28. Punnoose, E. A. *et al.* Expression profile of BCL-2, BCL-XL, and MCL-1 predicts pharmacological response to the BCL-2 selective antagonist venetoclax in multiple myeloma models. *Mol Cancer Ther* **15**, 1132–1144 (2016).
29. Alvarez, M. J. *et al.* Functional characterization of somatic mutations in cancer using network-based inference of protein activity. *Nat Genet* **48**, 838–847 (2016).
30. Jamaladdin, N. *et al.* Key pharmacokinetic parameters of 74 pediatric anticancer drugs providing assistance in preclinical studies. *Clin Pharmacol Ther* **114**, 904–913 (2023).
31. Rokita, J. L. *et al.* Genomic Profiling of Childhood Tumor Patient-Derived Xenograft Models to Enable Rational Clinical Trial Design. *Cell Rep* **29**, 1675-1689.e9 (2019).
32. Castillo-Ecija, H. *et al.* Prognostic value of patient-derived xenograft engraftment in pediatric sarcomas. *Journal of Pathology: Clinical Research* **7**, 338–349 (2021).
33. Kamili, A. *et al.* Accelerating development of high-risk neuroblastoma patient-derived xenograft models for preclinical testing and personalised therapy. *Br J Cancer* **122**, 680–691 (2020).
34. Akemi Kido, L. *et al.* Establishing a pediatric solid tumor PDX biobank for precision oncology research. *Cancer Biol Ther* **26**, (2025).
35. Hafner, M., Niepel, M., Chung, M. & Sorger, P. K. Growth rate inhibition metrics correct for confounders in measuring sensitivity to cancer drugs. *Nat Methods* **13**, 521–527 (2016).
36. Smith, M. A. *et al.* Lessons learned from 20 years of preclinical testing in pediatric cancers. *Pharmacol Ther* **264**, 108742 (2024).
37. Brenner, J. C. *et al.* PARP-1 inhibition as a targeted strategy to treat Ewing's sarcoma. *Cancer Res* **72**, 1608–1613 (2012).
38. Stewart, E. *et al.* Targeting the DNA repair pathway in Ewing sarcoma. *Cell Rep* **9**, 829–840 (2014).
39. Schafer, E. S. *et al.* Phase 1/2 trial of talazoparib in combination with temozolomide in children and adolescents with refractory/recurrent solid tumors including Ewing sarcoma: A Children's Oncology Group Phase 1 Consortium study (ADVL1411). *Pediatr Blood Cancer* **67**, 1–11 (2020).
40. Choy, E. *et al.* Phase II study of olaparib in patients with refractory Ewing sarcoma following failure of standard chemotherapy. *BMC Cancer* **14**, 1–6 (2014).
41. Takagi, M. *et al.* First phase 1 clinical study of olaparib in pediatric patients with refractory solid tumors. *Cancer* **128**, 2949–2957 (2022).
42. Tucker, E. R. *et al.* Combination Therapies Targeting ALK-aberrant Neuroblastoma in Preclinical Models. *Clinical Cancer Research* **29**, 1317–1331 (2023).
43. Zhang, Q. *et al.* ALK phosphorylates SMAD4 on tyrosine to disable TGF-β tumour suppressor functions. *Nat Cell Biol* **21**, 179–189 (2019).
44. Qu, H. *et al.* Smad4 suppresses the tumorigenesis and aggressiveness of neuroblastoma through repressing the expression of heparanase. *Sci Rep* **6**, 1–14 (2016).
45. Schubert, N. A. *et al.* Combined targeting of the p53 and pRb pathway in neuroblastoma does not lead to synergistic responses. *Eur J Cancer* **142**, 1–9 (2021).
46. McAleer, C. W. *et al.* On the potential of in vitro organ-chip models to define temporal pharmacokinetic-pharmacodynamic relationships. *Sci Rep* **9**, 1–14 (2019).
47. Smith, D. A., Di, L. & Kerns, E. H. The effect of plasma protein binding on in vivo efficacy: Misconceptions in drug discovery. *Nat Rev Drug Discov* **9**, 929–939 (2010).

48. Zhu, J. *et al.* Translational Pharmacokinetic/Pharmacodynamic Modeling and Simulation of Oxaliplatin and Irinotecan in Colorectal Cancer. *Pharmaceutics* **15**, (2023).
49. Pusch, F. F. *et al.* Elimusertib has anti-Tumor activity in preclinical patient-derived pediatric solid tumor models. *Mol Cancer Ther* **23**, 507–519 (2024).
50. Fernando, T. M. *et al.* Functional characterization of SMARCA4 variants identified by targeted exome-sequencing of 131,668 cancer patients. *Nat Commun* **11**, 1–13 (2020).
51. Surdez, D. *et al.* STAG2 mutations alter CTCF-anchored loop extrusion, reduce cis-regulatory interactions and EWSR1-FLI1 activity in Ewing sarcoma. *Cancer Cell* **39**, 810-826.e9 (2021).
52. Lin, G. L. & Monje, M. A protocol for rapid post-mortem cell culture of diffuse intrinsic pontine glioma (DIPG). *Journal of Visualized Experiments* **2017**, 1–8 (2017).
53. ElHarouni, D. *et al.* iTReX: Interactive exploration of mono- and combination therapy dose response profiling data. *Pharmacol Res* **175**, (2022).
54. Ritz, C., Baty, F., Streibig, J. C. & Gerhard, D. Dose-response analysis using R. *PLoS One* **10**, 1–13 (2015).
55. Love, M. I., Hogenesch, J. B. & Irizarry, R. A. Modeling of RNA-seq fragment sequence bias reduces systematic errors in transcript abundance estimation. *Nat Biotechnol* **34**, 1287–1291 (2016).
56. Korotkevich, G., Sukhov, V. & Sergushichev, A. fgsea: Fast Gene Set Enrichment Analysis. https://bioconductor.org/packages/fgsea (2023).
57. Liberzon, A. *et al.* Molecular signatures database (MSigDB) 3.0. *Bioinformatics* **27**, 1739–1740 (2011).
58. Dolgalev, I. msigdbr: MSigDB Gene Sets for Multiple Organisms in a Tidy Data Format, version 7.5.1. *https://cran.r-project.org/web/packages/msigdbr/index.html* (2022).
59. Ding, H. *et al.* Quantitative assessment of protein activity in orphan tissues and single cells using the metaVIPER algorithm. *Nat Commun* **9**, (2018).
60. Lachmann, A., Giorgi, F. M., Lopez, G. & Califano, A. ARACNe-AP: Gene network reverse engineering through adaptive partitioning inference of mutual information. *Bioinformatics* **32**, 2233–2235 (2016).
61. Margolin, A. A. *et al.* ARACNE: An algorithm for the reconstruction of gene regulatory networks in a mammalian cellular context. *BMC Bioinformatics* **7**, 1–15 (2006).
62. Zhang, W. *et al.* Comparison of RNA-seq and microarray-based models for clinical endpoint prediction. *Genome Biol* **16**, 1–12 (2015).

List of figures and legends

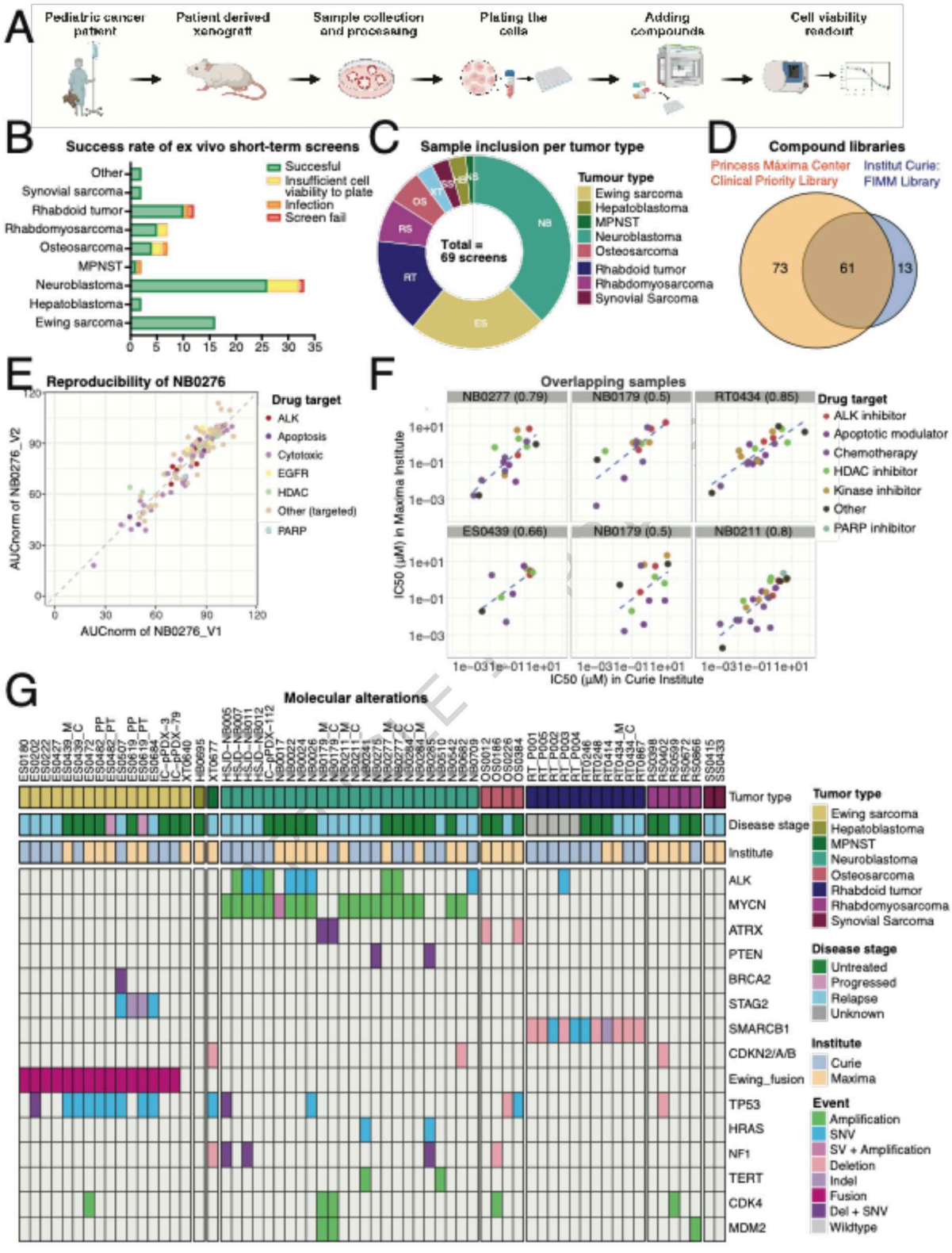
A
Pediatric cancer patient
Patient derived xenograft
Sample collection and processing
Plating the cells
Adding compounds
Cell viability readout
B
Success rate of ex vivo short-term screens
Other
Synovial sarcoma
Rhabdoid tumor
Rhabdomyosarcoma
Osteosarcoma
MPNST
Neuroblastoma
Hepatoblastoma
Ewing sarcoma
Succesful
Insufficient cell viability to plate
Infection
Screen fail
0 5 10 15 20 25 30 35
C
Sample inclusion per tumor type
Total = 69 screens
NB
ES
RT
RS
OS
KT
OS
MPNST
Tumour type
Ewing sarcoma
Hepatoblastoma
MPNST
Neuroblastoma
Osteosarcoma
Rhabdoid tumor
Rhabdomyosarcoma
Synovial Sarcoma
D
Compound libraries
Princess Máxima Center Clinical Priority Library
Institut Curie: FIMM Library
73
61
13
E
Reproducibility of NB0276
AUCnorm of NB0276_V2
AUCnorm of NB0276_V1
0 30 60 90 120
Drug target
ALK
Apoptosis
Cytotoxic
EGFR
HDAC
Other (targeted)
PARP
F
Overlapping samples
NB0277 (0.79)
NB0179 (0.5)
RT0434 (0.85)
ES0439 (0.66)
NB0179 (0.5)
NB0211 (0.8)
IC50 (µM) in Maxima Institute
IC50 (µM) in Curie Institute
1e−03 1e−01 1e+01
Drug target
ALK inhibitor
Apoptotic modulator
Chemotherapy
HDAC inhibitor
Kinase inhibitor
Other
PARP inhibitor
G
Molecular alterations
Tumor type
Disease stage
Institute
ALK
MYCN
ATRX
PTEN
BRCA2
STAG2
SMARCB1
CDKN2A/B
Ewing_fusion
TP53
HRAS
NF1
TERT
CDK4
MDM2
Tumor type
Ewing sarcoma
Hepatoblastoma
MPNST
Neuroblastoma
Osteosarcoma
Rhabdoid tumor
Rhabdomyosarcoma
Synovial Sarcoma
Disease stage
Untreated
Progressed
Relapse
Unknown
Institute
Curie
Maxima
Event
Amplification
SNV
SV + Amplification
Deletion
Indel
Fusion
Del + SNV
Wildtype

Figure 1: Ex vivo drug sensitivity profiling is feasible for a broad range of high-risk solid tumors. *A) Schematic representation of drug screening protocol. B) Success rate of ex vivo drug screens by tumor type, showing the proportion of samples with successful screens, samples with insufficient viability for plating, and samples with unsuccessful screens due to either infection or screening failure. C) Donut plot showing the cohort overview of ex vivo direct screens per tumor type. D) Number of compounds in drug libraries of the Princess Máxima Center (orange), Curie Institute (blue) and the number of overlapping compounds (brown). E) Scatterplot of drug sensitivity (AUC_{norm}) for ex vivo cultures from two distinct PDX samples of the same patient sample (NB0276) that were received two months apart and followed the same protocol in Máxima. Each dot represents the AUC_{norm} per compound, colored by drug target. Pearson correlation coefficient = 0.95. F) Comparison of drug sensitivities (AUC_{norm}) of overlapping patient samples screened in both institutes. For each patient sample, a scatterplot of IC50 values is shown (includes only those compounds for which IC50 was reached in both institutes). Each dot represents a compound, colored by drug target. Pearson correlation coefficients are indicated between brackets. G) Oncoplot depicting the molecular landscape of PDX models included in the cohort, showing key targetable genetic alterations. MPNST = malignant peripheral nerve sheath tumor; _M = screened in the Máxima institute; _C = screened in Institut Curie; _PP = PDX of primary tissue; _PT = PDX of progression under treatment tissue.*

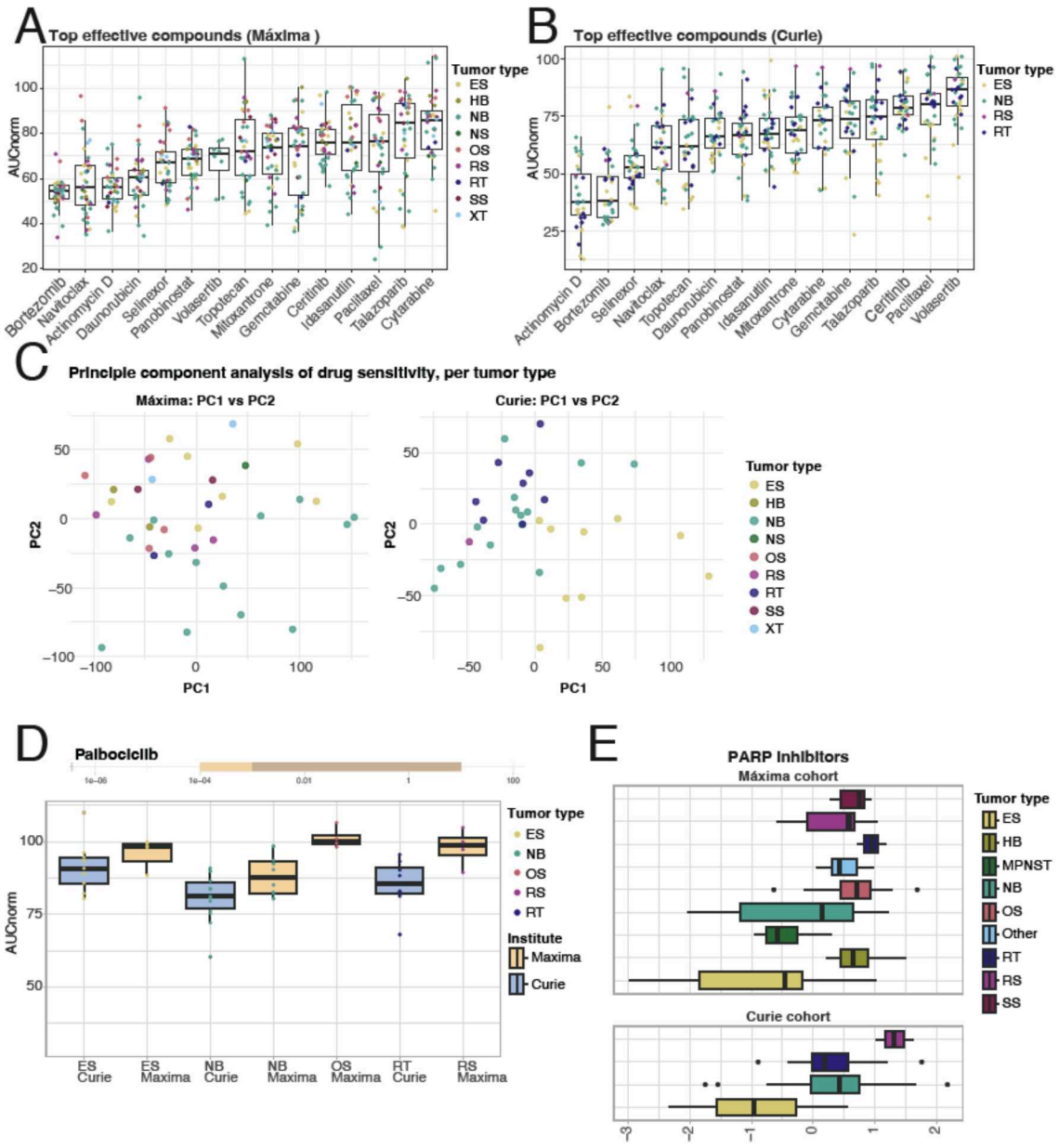

Figure 2: Ex vivo drug sensitivity profiling to reliably predict tumor-type specific response in two cohorts. *A-B) Boxplot representing the top 15 performing compounds based on AUCnorm in the Máxima (A) and Curie (B) cohorts. Only compounds tested in both institutes are included. Each dot represents an individual sample, colored according to the tumor type. For all box plots: the box represents the interquartile range (IQR), with the median (50th percentile) indicated by the horizontal line inside the box. The whiskers extend to 1.5 times the IQR, with data points outside this range considered as outliers and shown as individual*

points. C) Principal component analysis (PCA) showing PCA1 versus PCA2 on the drug response profiles, each dot represents a sample, colored by tumor type. D) Tumor-type specific sensitivity for palbociclib is shown in the two cohorts. Dose ranges (in µM) are indicated on top for both cohorts (Máxima in orange, overlapping in brown). Box plots show AUC_{norm} scores per tumor type, per cohort. Orange boxes represent the Máxima cohort and blue boxes represent Curie. Neuroblastoma samples demonstrate specific sensitivity for palbociclib. E) Tumor-type specific sensitivity for PARP inhibitors (olaparib and talazoparib) tested in two cohorts. Box plots show Z-scores (based on AUC_{norm}) per tumor type, for the Máxima (top) and Curie (bottom) cohorts. Ewing sarcomas demonstrate specific sensitivity for PARP inhibitors. A lower Z-score represents greater sensitivity compared to the other samples, the higher the Z-score, the less sensitive the sample is for this compound.

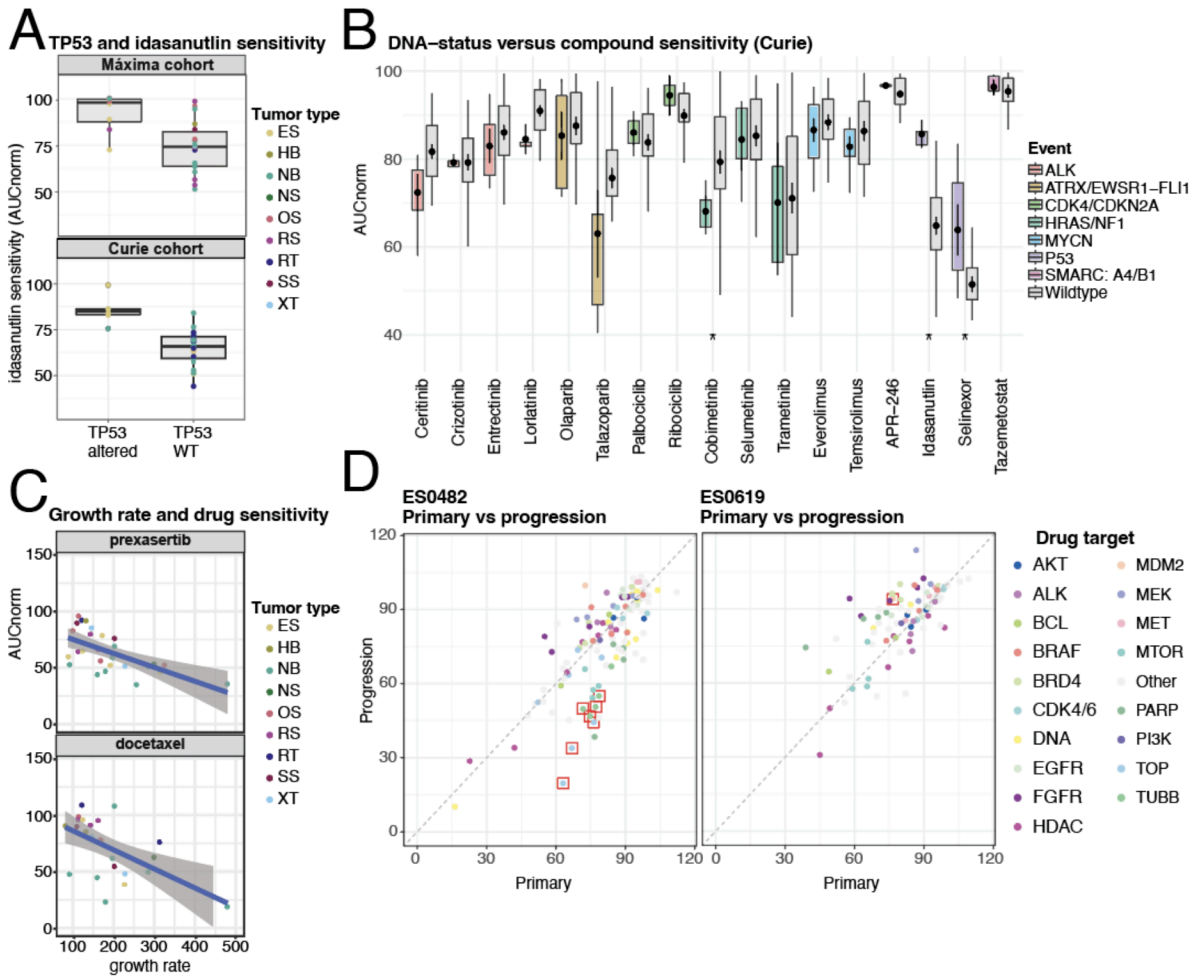

Figure 3: Ex vivo drug sensitivity profiling to identify associations with drug response and ex vivo growth rate, and to identify timepoint specific therapeutic windows *A) Box plots representing AUC_{norm} for idasanutlin of patients harboring wild type (WT) TP53 (right) and samples harboring homozygous TP53-inactivating events (left) in both cohorts. Samples are colored by tumor type. B) Boxplots representing sensitivity (AUC_{norm}) in Curie for targeted compounds, where colored boxes represent the ex vivo cultures from PDX models with genetic alterations colored by the alteration targeted by that compound (colored = altered, grey = wild type). Stars show a significant difference ($p < 0.05$) in drug response in the altered versus wild type samples (grey stars: these alterations are only present in neuroblastoma, and significance did not hold in neuroblastoma only analyses). C) Scatter plot that shows correlation of growth rate and AUC_{norm} for prexasertib and docetaxel. Each dot represents a sample, colored per tumor type. D) Drug sensitivity for two Ewing sarcoma patients in two timepoints (primary and progression samples), left represents ES0482 and right represents ES0619. Each dot represents the AUC_{norm} of a compound, which is colored by its target subtype. Compounds that are highlighted by the red boxes: topoisomerase and tubulin inhibitors are influenced by the growth rate in ES0482 and idasanutlin, which is influenced by an acquired homozygous TP53-inactivation in ES0619.*

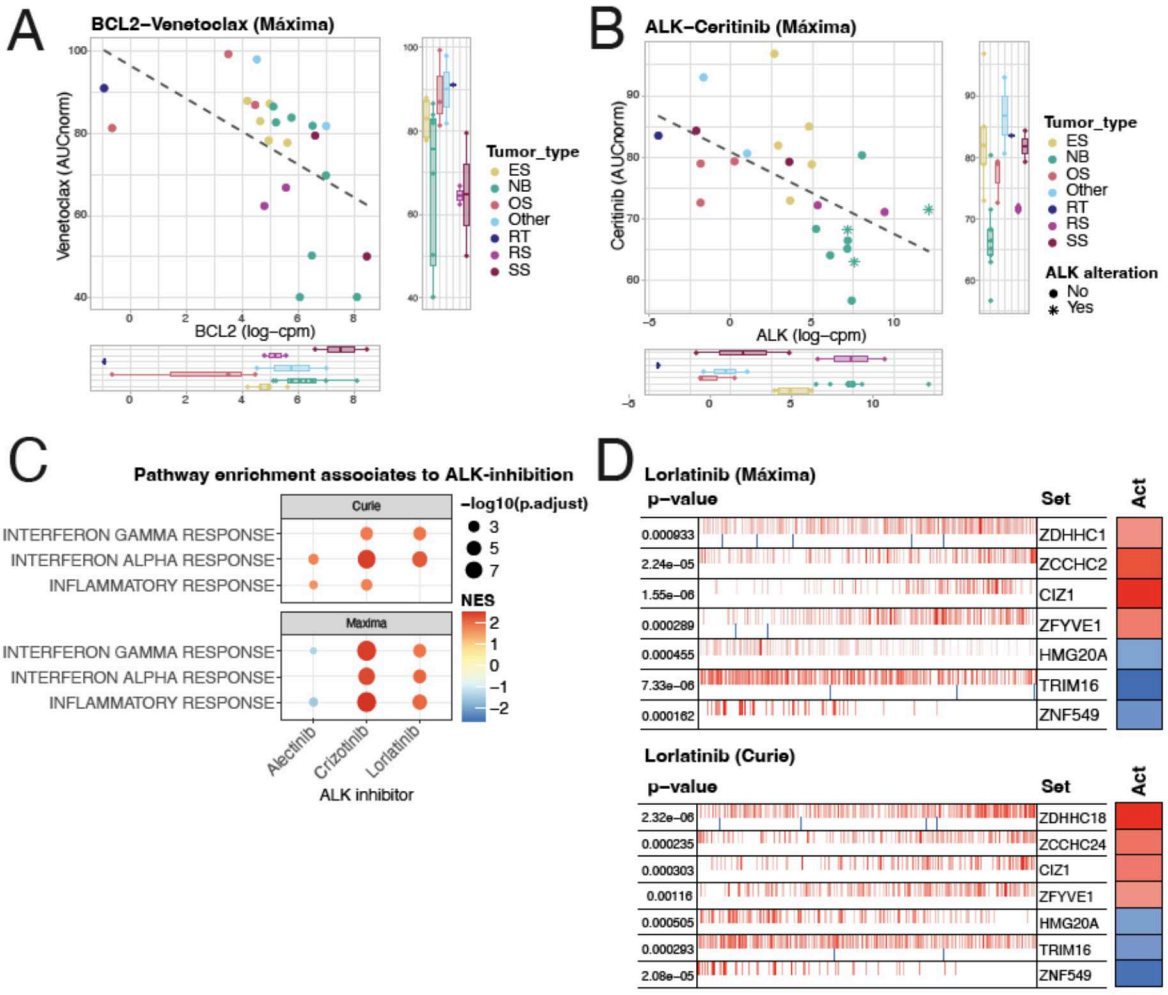

Figure 4: RNA expression and pathway analyses associated with ex vivo drug sensitivity of targeted compounds. *A) Scatterplot representing BCL-2-expression versus drug sensitivity for BCL-2-inhibitor venetoclax in the Máxima cohort (n = 23). Samples are colored by tumor type, boxplots represent BCL-2-expression across tumor types (bottom) or* AUC_{norm} *across tumor types (right). B) Scatterplot representing ALK-expression versus drug sensitivity for ALK-inhibitor ceritinib in the Máxima cohort (n = 24). Samples are colored by tumor type, shapes resemble ALK-genetic status (circle: wild type; star: altered), boxplots represent ALK expression across tumor types (bottom) or* AUC_{norm} *across tumor types (right). C) Dot plot showing pathway enrichment associated with sensitivity to alectinib, crizotinib, and lorlatinib in neuroblastoma ex vivo screens (Máxima: n = 8, Curie: n = 11). Pathways shown are those significantly enriched for at least one drug in either cohort; top 15 pathways with overlap across cohorts are*

highlighted, although the enrichment direction may differ between drugs or cohorts. Dot color indicates the Normalized Enrichment Score (NES) (red = positive enrichment, blue = negative); dot size reflects statistical significance (–log_{10} adjusted p-value), with larger dots indicating greater significance. MES = mesenchymal. D) Overlapping MRs associated with sensitivity to lorlatinib in neuroblastoma ex vivo screens. VIPER analysis results for the Máxima and Curie cohorts, highlighting TFs whose regulatory activity is significantly (padj. < 0.05) associated with drug sensitivity and shared between both cohorts for lorlatinib. Each row shows a TF inferred as an MR based on the coordinated differential expression of its target genes (regulon). The barcode plot (middle panel) shows the projection of each MR's activated (red) and repressed (blue) target genes along the gene expression signature (GES), ranked from the most downregulated (left) to the most upregulated (right) in drug-sensitive tumors. The heatmap (right panel) shows the MR Activity Score (Act) which indicates inferred regulatory activity (red = activation; blue = repression). Color intensity reflects the strength of activation or repression, with more saturated colors indicating greater inferred activity differences.

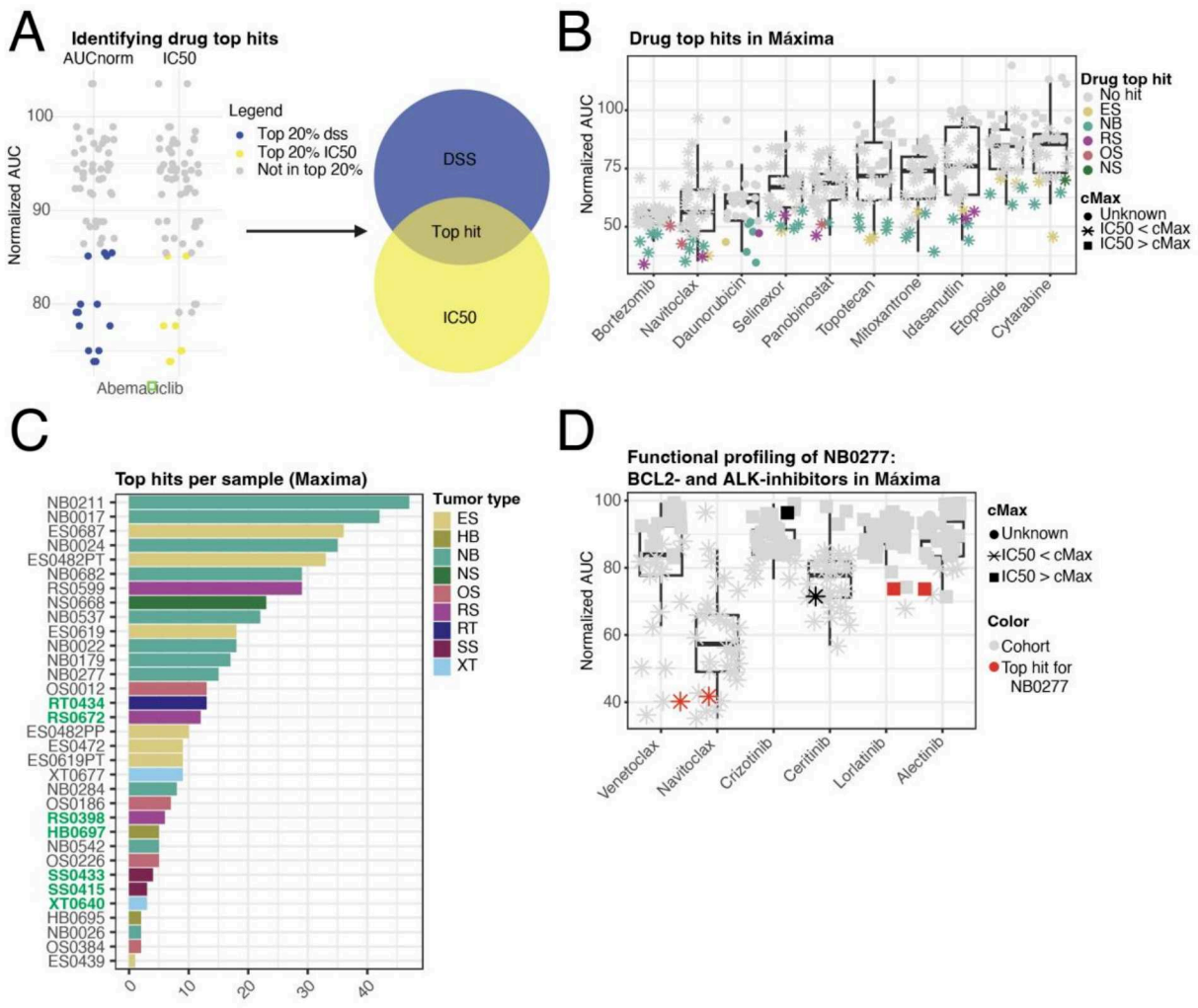

Figure 5: Ex vivo drug sensitivity profiling to complement molecular profiling in guiding clinical decisions

A) Drug top hits are identified per compound, as patients whose AUC_{norm} and IC50 both fell within the 20% most responsive quantile. In this case, IC50 values for abemaciclib were not reached in all samples, therefore the top 20% consists of seven samples (versus fourteen in AUCnorm). B) Boxplots representing 10 most effective compounds in Máxima. For drug top hits, samples are colored by tumor type. The shape of each datapoint represents if the IC50 is lower than Cmax (star), higher then Cmax (square) or if Cmax is unknown/ IC50 is undetermined (circle). C) Number of top hits found for samples included in the Máxima cohort. Bold and green sample names represent samples for which molecular profiling failed to identify a targetable alteration. D) Ex vivo drug sensitivity (normalized AUC) in the Máxima cohort exemplifying only

BCL2- and ALK-inhibitors. Red datapoints resemble normalized AUCs of drug top hits for NB0277, black datapoints resemble normalized AUCs of compounds not found as drug top hit for NB0277, grey datapoints resemble the rest of the cohort.